Experimental Evidence for and Prediction of Micromixing Effects in Precipitation

Bruno Marcant and René David
Laboratoire des Sciences du Génie Chimique, CNRS - ENSIC - INPL, F 54001 Nancy Cedex, France

The influence of micromixing on precipitation is predicted qualitatively for batch or semibatch precipitations by means of a simplified mixing model, which considers primary nucleation as the main process affected significantly by hydrodynamics. Unwanted micromixing effects are avoided to a maximum in a batch configuration designed to have a volume mixing ratio α close to unity. Using a semibatch precipitator or a batch with a high α value dramatically accentuates mixing interactions. For mixing, changing the feed point location is shown to have much stronger influence than changing the stirring speed and constitutes an efficient test of micromixing. Experimental evidences for these conclusions have been established for calcium oxalate monohydrate batch precipitation. In particular, the early seconds of the reaction (when mainly primary nucleation occurs) have been demonstrated as conditioning the subsequent behavior of the precipitation, even for induction times of a few minutes.

Introduction

Precipitation is a widely used industrial chemical operation which has been found to be greatly affected by hydrodynamics in both laboratory equipment and in production plants. Micromixing, or mixing at the microscopic scale, has been shown to be primarily responsible for this influence, mainly affecting crystal size distribution (CSD).

The reason is that precipitation involves fast chemical events whose reaction times are of the same order of magnitude as the characteristic time for the mixing steps leading to homogenization of concentration in the apparatus. This leads to a segregation process, and the resulting local concentration gradients influence the subsequent course of the precipitation.

The purpose of this article is to demonstrate experimental situations that prevent batch or semibatch precipitation results being obscured by micromixing effects as much as possible. A simplified theoretical model is used to define these situations, which are further validated by experiments on the precipitation of calcium oxalate monohydrate.

The use of these simple concepts is recommended especially to those interested in studies of crystallization kinetics. Indeed, as kinetic models generally neglect mixing problems, they will then be sure that experimental measurements effectively correspond to the crystallization kinetics and not to an interaction of them with the mixing processes.

Basic Crystallization

Crystallization of a chemical species occurs in a solution if the concentration of the solute exceeds its solubility. This excess represents the driving force for crystallization and is called supersaturation $s = C - C^*$ or in the dimensionless form $S = C/C^* - 1$ (Mersmann and Kind, 1988).

Precipitation is a crystallization process, in which a high initial supersaturation is created by a chemical reaction between soluble substrates, generally ions. Considering the simple case of two reactants A and B, precipitation may occur either by direct integration $A + B \rightleftharpoons P$ (solid) or by a sparingly soluble intermediate that crystallizes $A + B \rightleftharpoons R \rightleftharpoons P$ (solid).

Crystallization involves the following main processes:

Nucleation. Solid formation starts with the appearance of very small crystals called nuclei. This process involves mainly homogeneous primary nucleation during the first stage of precipitation where there are high values of supersaturation and heterogeneous secondary nucleation when the molar concentration of crystals becomes significant (Nyvlt et al., 1985).

Growth. Nuclei or crystals grow by continuous acquisition of solute as long as supersaturation remains positive. It is frequently described as a combination of two steps: mass transfer through the crystal boundary layer and then integration to the crystal lattice (Marchal et al., 1988).

Ostwald Ripening. According to the Gibbs-Thomson-Ostwald-Freundlich law, crystals smaller than the limit size of nuclei have negative local supersaturation resulting in their dissolution (Kulov et al., 1983; Matz, 1985).

Agglomeration and Aggregation. Binary encounters of crystals and subsequent adhesion also lead to growth (Nyvlt and Karel, 1985).

Mixing

We consider the mixing of a given volume of a species B in a larger volume of a species A. From the point of view of fluid mechanics, this involves the following four predominant, consecutive steps (Beek and Miller, 1959):

- Macroscopic shearing of the inlet flow B due to the average velocity of the fluid A inside the precipitator that leads to the distribution of packets of B in A.
- Turbulent diffusion involving erosion and division of the packets of B.
- Laminar stretching of the latter when they reach very small dimensions, which is completed by the formation of vortices and eddies.
- Molecular diffusion of B in A when the previous structures are sufficiently small.

More generally, progressive mixing of B in A can be represented by two consecutive processes (David and Villermaux, 1987): initial macromixing involving equalization of the average concentration in space and subsequent micromixing of the segregated state representative of the local concentration fluctuations.

Interactions are to be expected with the reaction process when these mixing effects take place on a time scale equal to or greater than the characteristic reaction time. This is effectively the case with precipitation, since some crystallization steps such as primary nucleation are frequently fast or very fast.

Perfect mixing is generally achieved within a few seconds. Consequently, the competition between reaction and mixing is likely to occur only within a short period of time following the feed introduction. For a batch precipitator, it occurs only once at the introduction of the reactant. On the other hand, for semibatch and continuous reactors, it proceeds as long as they continue to be supplied with reactants (if at least one of the reaction rates remain sufficiently high).

Another aspect of mixing is the rotation speed of the stirrer. Its influence on diffusional growth has long been recognized (Nyvlt et al., 1985). Nevertheless, this effect seems to be less important.

Literature Survey

In 1958, Danckwerts first underlined the importance of quality of mixing on precipitation. Nevertheless, a numerical study of two extreme mixing conditions (maximum mixedness and complete segregation) in a continuous, mixed-suspension, mixed-product-removal (MSMPR) crystallizer was not presented until 1969 (Becker and Larson). Garside and Tavare (1985) studied a similar situation for the case of precipitation where nucleation rates are higher than in crystallization since supersaturations are larger.

Following these initial investigations, the problem of the interactions between mixing and crystallization or mixing and precipitation have been studied for continuous processes (Tavare, 1986) in various chemical systems. Examples of potassium dichromate (Desai et al., 1974) and barium sulfate precipitations (Pohorecki and Baldyga, 1988; Fitchett and Tarbell, 1990) are of particular interest.

The batch and semibatch cases have been investigated even less. Pohorecki and Baldyga (1983) made an experimental study of the influence of stirring speed and initial reactant concentrations on the behavior of barium sulfate batch precipitation. Experimental studies by Söhnel and Mullin (1987) on Ag_2WO_4, $CaWO_4$ and $SrWO_4$, and by Aslund and Rasmuson (1989) on benzoic acid showed the importance of the stirring rate on batch precipitation. For single- or double-jet, semibatch precipitators used for barium sulfate or dimethylglyoxime precipitation, Kuboi et al. (1986) demonstrated both the influence of the feed position and the intensity of mixing on the CSD. Recently, Tosun (1989) presented similar experimental work on barium sulfate.

Villermaux and David (1988) simulated the evolution of precipitation and the subsequent CSD in single- or double-jet, semibatch reactors by means of a simple IEM (interaction by exchange with the mean) model, and a more sophisticated approach that took into account the progressive incorporation of the incoming fluid into the bulk (David and Villermaux, 1987, 1989).

Finally, using a similar model (Baldyga and Bourne, 1989), Baldyga et al. (1990) interpreted experimental results of barium sulfate semibatch precipitation in light of such factors as impeller speed, reactant concentrations, stoichiometric ratio, volume ratio of reactant solutions, and feed position.

Evaluation of Possible Mixing Effects

In this section, we consider precipitation resulting from a chemical reaction between two ionic solutions A and B with the respective concentrations C_A^i and C_B^i.

Let us imagine the following mixing scheme, which accounts both for batch and semibatch single jet precipitations in a stirred tank (Figure 1): a volume V_B^i of reactant B is added into a volume V_A^i of reactant A. Initial concentrations C_A^i and C_B^i are fixed such that the number of moles of reactants remains constant during the first seconds corresponding to the mixing processes. After complete and perfect mixing, the concentrations would be C_B^o and C_A^o, respectively. Defining

$$\alpha = \frac{V_A^i}{V_B^i}, \tag{1}$$

these concentrations are given by:

$$C_A^o = C_A^i \frac{\alpha}{1+\alpha} \text{ and } C_B^o = C_B^i \frac{1}{1+\alpha}, \tag{2}$$

and the initial mean supersaturation is estimated from:

$$\bar{S}^o = \frac{C_A^o C_B^o}{P_s} - 1 = \frac{C_A^i C_B^i}{P_s\left(2+\alpha+\frac{1}{\alpha}\right)} - 1 \tag{3}$$

However, the primary nucleation process is usually so rapid that it may begin before the concentrations in the tank are

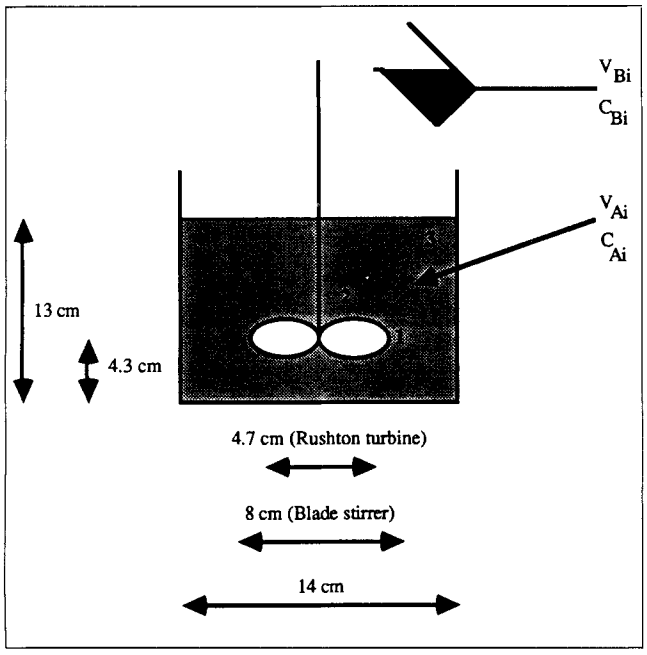

Figure 1. Mixing scheme.

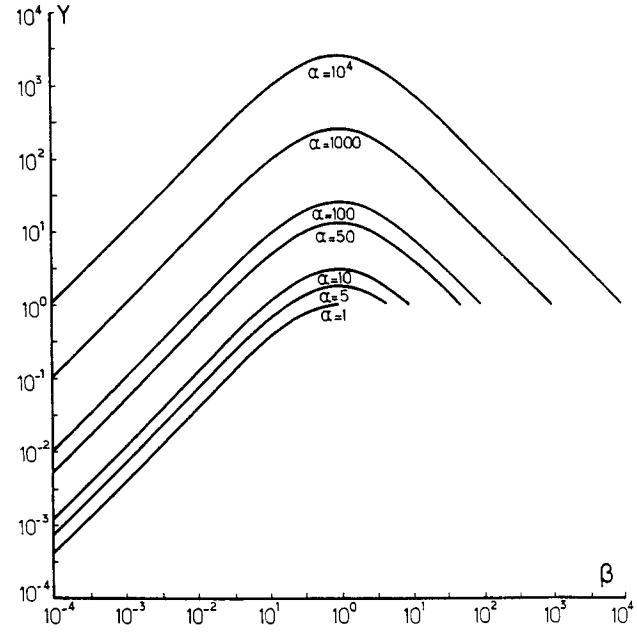

Figure 2. *Y* ratio vs. mixing ratio β.

fully homogenized. This is not contradictory with the previous assumption, since nucleation does not consume large amounts of solute. Thus, as far as nucleation is concerned, an overall description of the composition of the reactor contents after perfect mixing is not sufficient. It is necessary to include local mixing effects to determine the influence of local supersaturation fluctuations on the rate of primary nucleation.

Simplified micromixing model

The mixing process depicted in the introduction as involving four steps is rather complex and implies a complicated contacting between the reactive species. The most important step is the final mixing on the molecular scale, that is, micromixing, as supersaturation and the primary nucleation process only start after molecular contacting of both reactants.

In fact, most of A and B molecules reach this state before the complete spatial distribution of reactant B into reactant A. We, therefore, assume that during this final mixing step, instead of being contacted with the entire volume of A, the feed volume V_B^i is initially mixed at the molecular level with a smaller volume $V_A'^i$ of A, where $V_A'^i = \beta V_B^i$ (with $\beta \leq \alpha$).

This simple model is similar in its principle to the engulfment or incorporation model proposed by Baldyga and Bourne (1984), the only difference being that, for the sake of simplicity, no time scale is defined for the partial mixing processes.

Influence on local supersaturation

The simplest representation of micromixing consists in assuming V_B^i is first contacted on the molecular scale with a reduced volume $V_A'^i = \beta V_B^i$, with $\beta \leq \alpha$. Hence, the respective concentrations of reactants A and B after mixing in the volume $V_A'^i + V_B^i$ are:

$$C_A'^o = C_A^i \frac{\beta}{1+\beta} \text{ and } C_B'^o = C_B^i \frac{1}{1+\beta} \tag{4}$$

Thus, the local initial supersaturation in this volume is:

$$S^o = \frac{C_A'^o C_B'^o}{P_s} - 1 = \frac{C_A^i C_B^i}{P_s\left(2+\beta+\frac{1}{\beta}\right)} - 1 \tag{5}$$

and

$$Y = \frac{S^o+1}{\bar{S}^o+1} = \frac{2+\alpha+\frac{1}{\alpha}}{2+\beta+\frac{1}{\beta}} \tag{6}$$

Whereas α is fixed by the experimental procedure, β depends only on the mixing process: good macro- and micromixing leads to β values close to α. As the problem is symmetrical with respect to A and B, only the case $\alpha \geq 1$ will be examined. Figure 2 presents the variations of the ratio Y with β at constant α values.

In any case, full homogeneity ($Y = 1$) is achieved for identical values of α and β. For high α values, Y reaches its maximum when β is unity. This means that in incomplete mixing situations, very high intermediate local supersaturation may be achieved. When α is not very different from 1 (mixing of volumes of the same order of magnitude), defective mixing always leads to $Y \leq 1$.

Influence on primary nucleation rate

The driving force for primary nucleation is $S+1$, and the overall nucleation rate is:

$$r_N = A_N \exp\left(\frac{-B_N}{\log_e^2(S+1)}\right) \tag{7}$$

Defining a nucleation efficiency in the volume $(V_A^i + V_B^i)$,

$$\zeta = \frac{(V_A'^i + V_B^i)(\text{nucleation rate with nonperfect mixing})}{(V_A^i + V_B^i)(\text{nucleation with perfect mixing})}$$

makes it possible to evaluate the consequences of relation 6 on primary nucleation in the whole volume in the initial moments of the precipitation.

In the batch precipitation case, since no nucleation occurs outside the volume $V_A'^i + V_B^i$, the nucleation efficiency is derived directly from Eqs. 3, 5, and 7:

$$\zeta = \frac{1+\beta}{1+\alpha} \frac{\exp\left[\dfrac{-B_N}{\log_e^2\left\{(\overline{S^o}+1)\dfrac{\left[2+\alpha+\dfrac{1}{\alpha}\right]}{\left[2+\beta+\dfrac{1}{\beta}\right]}\right\}}\right]}{\exp\left[\dfrac{-B_N}{\log_e^2(\overline{S^o}+1)}\right]} \tag{8}$$

On the other hand, estimation of ζ is more complex for a semibatch single jet precipitation, since the initial mean supersaturation and the ratio α changes as long as addition of reactant B continues. Let us describe this operation by considering a dropwise addition of B consisting of m fractions or drops with a total volume V_B^i.

After the first drop has been added:

$$V_{A1} = V_A^i, \quad V_{B1} = \frac{V_B^i}{m},$$

so

$$\alpha_1 = \frac{mV_A^i}{V_B^i} = m\alpha \text{ and } \overline{S_1^o} = \frac{C_A^i C_B^i}{P_s\left(2+m\alpha+\dfrac{1}{m\alpha}\right)} - 1 \tag{9}$$

If the total addition time is assumed to be short enough to avoid significant consumption of the reactant by crystal growth after addition of the *j-st* drop we have:

$$V_{Aj} = V_A^i + (j-1)\frac{V_B^i}{m}, \quad V_{Bj} = \frac{V_B^i}{m},$$

so

$$\alpha_j = m\alpha + j - 1 \text{ and } \overline{S_j^o} = \frac{C_A^i C_B^i}{P_s\left(2+\dfrac{\alpha m}{j}+\dfrac{j}{\alpha m}\right)} - 1 \tag{10}$$

Consequently, α_j is always larger than α and increases with j, while $\overline{S_j^o}$ is smaller than $\overline{S^o}$ and increases with j.

This formalism proves that relation 8 is also applicable to the semibatch configuration, but with higher values of the volume ratio and lower values of the initial mean supersaturation than in the batch case.

Figures 3 and 4 illustrate the different cases resulting from relation 8. The (B_N, $\overline{S^o}$) plane may be separated into three sections:

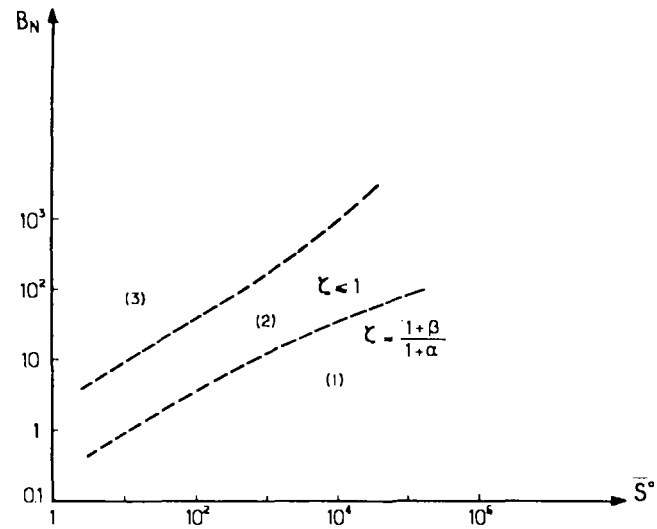

Figure 3. Different regions of nucleation efficiency in the (B_N, $\overline{S^o}$) plane.

Section 1. $\overline{S^o}$ is high, B_N is small, so $r_N \cong A_N$ and $\zeta \cong (1+\beta)/(1+\alpha) \leq 1$.

Section 2. $\zeta \leq 1$, but the relation above does not apply.

Section 3. $\zeta \geq 1$ is possible when B_N is high and $\overline{S^o}$ is relatively low.

In any case, $\zeta \cong 1$ for $\alpha \cong \beta$, when perfect macro- and micromixing are achieved.

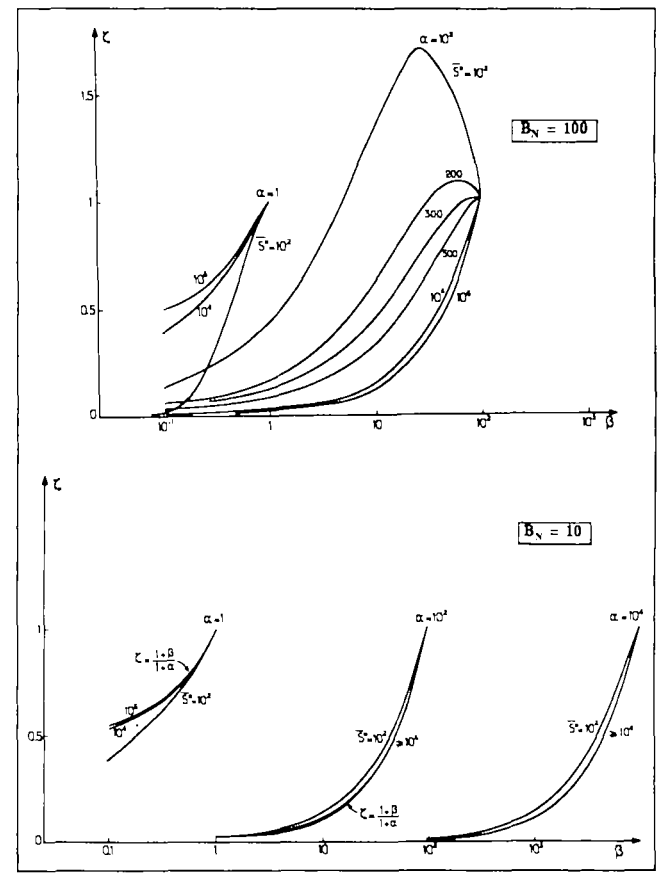

Figure 4. Nucleation efficiency ζ vs. mixing ratio β.

From the previous calculations, three conclusions may be drawn:

1. A small volume available for nucleation generally makes up for the high nucleation rates resulting from high intermediate local supersaturations in situations of incomplete mixing ($\beta \leq \alpha$); consequently, $\zeta \leq 1$ usually obtains.

It may also be possible that ripening (Nyvlt et al., 1985) of the crystals initiated under these high supersaturations occurs very rapidly. When complete and perfect mixing are achieved, supersaturation is much lower and these small crystals become thermodynamically unstable and are doomed to disappear.

2. To perform valid kinetic studies, it is necessary to operate with $\zeta \cong 1$. This can be achieved only if the local volume ratio β during mixing on the molecular scale equals the overall volume ratio α.

$\beta \cong \alpha$ certainly holds for batch precipitations with α close to 1: for such precipitations, molecular mixing between the reactants takes place when the added fluid has been dispersed through the whole tank (in other words, with good macromixing), allowing all A to be contacted with B. In fact, in the first three stages of the mixing process, the contacting of both reactants at the molecular scale is not achieved and so no primary nucleation occurs.

Other mixing situations, such as batch precipitations with high α volumes and semibatch single jet precipitations, will lead to partial contact at the molecular scale between the reactants before micromixing is completed. According to Baldyga and Bourne (1984), the local volume ratio for molecular mixing by vorticity and diffusion is about $\beta = 1$ for semibatch, single-jet, stirred reactors. Thus, α is larger than β, and a segregation process at the molecular level is likely to occur.

3. Mixing effects are accentuated in precipitations having high α values. For this purpose, semibatch, single-jet precipitators may be employed, but also batch precipitations with addition of a small volume V_B^i of highly concentrated B with respect to V_A^i. In both cases, β increases from about 1 at the beginning of the diffusive mixing step up to α. Thus, nucleation efficiency is not always near 1, implying that the number of crystals produced and the final CSD differ from that obtained under perfect-mixing conditions.

Influence of the stirring speed vs. the feed point

Up to this point we have discussed only the initial seconds of the precipitation and the micromixing process in batch or semibatch reactors. In fact, two factors are likely to affect mixing conditions during this short period: the feed point location and the stirrer speed.

The influence of the second parameter continues as long as precipitation proceeds. Thus, while only the primary nucleation is affected by the feed point location, the rates of primary nucleation, secondary nucleation, diffusional growth and agglomeration increase with stirring intensity. The resulting effects of these two factors on physical values such as the number of crystals per unit volume N_c, the average diameter D of the crystals, and the overall reaction rate r are summarized in Table 1.

An increase of stirring speed with a fixed feed point has different effects on N_c and D, while r increases. This has been already confirmed experimentally by Tosun (1989) for barium sulfate precipitation.

On the other hand, when the stirring speed is kept constant, moving the feed addition point from one zone to another where the turbulence level is higher influences the primary nucleation only. This is because growth, agglomeration, and even secondary nucleation are slower processes, and their rates are integrated over the entire recirculation flow of the reactor. Consequently, higher values of N_c and r as well as lower values of D are expected in this situation.

Effects are revealed to be more drastic in the second case. That is why the influence of the feed addition point may be much more important than the stirring speed as far as mixing is concerned.

Therefore, changing the feed point for a constant stirring speed can be a test of the state of micromixing in a reactor. If different addition points are used and no modifications are observed in the conversion curve or CSD, then there is no influence of micromixing on the outcome of the reaction. On the contrary, experiments of this kind with varying stirring speeds cannot be as easily interpreted, since there is competition between contradictory effects (Table 1). Only the first procedure leads to firm conclusions. In particular, the presence of long induction times in batch precipitation does not ensure that results do not depend on micromixing.

These conclusions are valid when primary nucleation is the only process that is sufficiently fast to be influenced by micromixing, that is, when no significant consumption of reactants takes place during the first seconds of precipitation corresponding to the mixing stage. In our experimental investigation we used different initial concentrations to verify this condition (see Figure 5a, for example). This would not be the case with forced initial concentrations, since the subsequent higher primary nucleation rate would produce crystals in a sufficient quantity much more rapidly so that the overall crystalline surface available would allow a large conversion of reactants by growth before the end of the mixing step. In this case, our previous simplified model would not be suitable.

Table 1. Influence of Better Mixing on Precipitation Processes*

	Rapid Local Process	Slow Processes Averaged over the Tank				Overall Effect
	Primary Nucleation	Secondary Nucleation	Growth by Integration	Diffusional Growth	Agglomeration	
Same Feed Point, Increasing Stirring Speed	Enhanced $N_c\nearrow$, $D\searrow$, $r\nearrow$	Enhanced $N_c\nearrow$, $D\searrow$, $r\nearrow$	No influence $N_c\rightarrow$, $D\rightarrow$, $r\rightarrow$	Enhanced $N_c\rightarrow$, $D\nearrow$, $r\nearrow$	Enhanced $N_c\searrow$, $D\nearrow$, $r\rightarrow$	N_c? D? $r\nearrow$
Same Stirring Speed, Addition in a More Turbulent Zone	Enhanced $N_c\nearrow$, $D\searrow$, $r\nearrow$	No influence $N_c\rightarrow$, $D\rightarrow$, $r\rightarrow$	No influence $N_c\rightarrow$, $D\rightarrow$, $r\rightarrow$	No influence $N_c\rightarrow$, $D\rightarrow$, $r\rightarrow$	No influence $N_c\rightarrow$, $D\rightarrow$, $r\rightarrow$	$N_c\nearrow$ $D\searrow$ $r\nearrow$

*N_c = number of crystals per unit volume; D = crystal mean diameter; r = overall crystallization rate

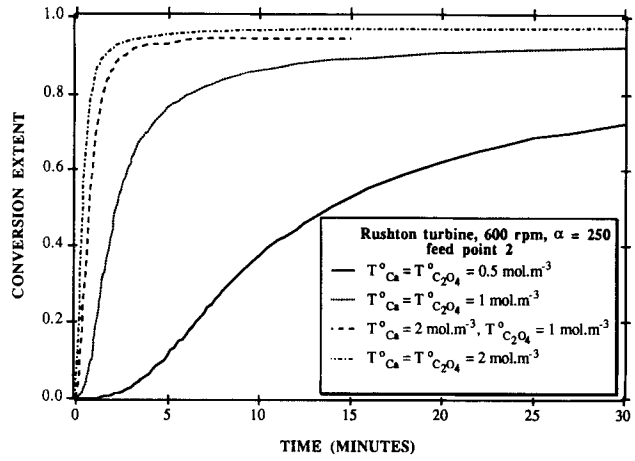

Figure 5a. Extent of conversion as a function of time at four total initial concentrations.

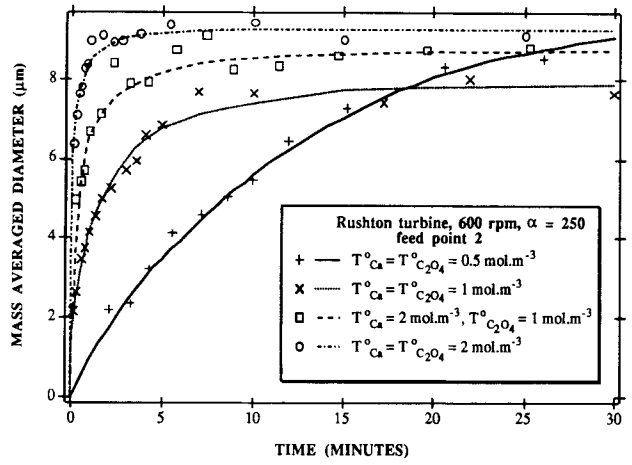

Figure 5b. Mass-averaged diameter as a function of time at four total initial concentrations.

Finally, it is necessary to keep in mind that the above discussion is based on expression 7 for primary nucleation, and Garside (1985) has discussed its validity.

Experimental Investigation

The considerations given above concerning the effects of imperfect mixing have been applied to an experimental study of the batch precipitation of calcium oxalate monohydrate.

This reaction involves two ionic species in solution (Ca^{2+}, $C_2O_4^{2-}$) and one soluble complex (CaC_2O_4), with the association constant K_A (Gardner, 1975; Brecevic et al., 1986) and the solubility product P_s (Tomazic and Nancollas, 1979) at 25°C:

$$K_A = \frac{a_{CaC_2O_4}}{a_{Ca^{2+}} a_{C_2O_4^{2-}}} = 1.537 \text{ m}^3 \cdot \text{mol}^{-1} \tag{11}$$

$$P_s = a^*_{Ca^{2+}} a^*_{C_2O_4^{2-}} = 1.66 \times 10^{-3} \text{ mol}^2 \cdot \text{m}^{-6} \tag{12}$$

Precipitation was performed in a 2-dm³ batch crystallizer, mechanically stirred with a Rushton turbine or a pitched-blade stirrer (some dimensions are indicated in Figure 1), and the temperature was kept constant at 25 ± 0.1°C by a double-wall jacket. The initial reacting solutions of calcium chloride and potassium oxalate were prepared with deionized water, adjusted to pH = 7 and then filtered on 0.22-μm millipore filters.

Initiation was always carried out by rapid addition of a small pulse of a volume V_B^i of calcium chloride into a volume V_A^i of potassium oxalate, so as to reach initial mean supersaturations (Eq. 3) within the range 40 to 350. Three locations of the feed point are usually used (see Figure 1). Inversion of the method of addition was shown to have no influence on the crystallization. This can be explained by the fact that, as calcium oxalate is a 1-1 crystal, the mixing and reaction are completely symmetrical with respect to Ca^{2+} and $C_2O_4^{2-}$ ions.

Provision was made for measurement of the liquid and solid characteristics as a function of time.

Liquid phase

The composition of the liquid phase was monitored using a conductimeter with very rapid response time (see the Appendix).

Assuming perfect mixing at the beginning of the precipitation, the total initial concentrations of calcium and oxalate are given by:

$$T^o_{Ca} = C^o_{Ca^{2+}} + C^o_{CaC_2O_4}$$

and

$$T^o_{C_2O_4} = C^o_{C_2O_4^{2-}} + C^o_{CaC_2O_4} \tag{13}$$

As dilute solutions were used, it is necessary to use activities rather than concentrations for good estimation of the mean supersaturation:

$$\overline{S^o} = \frac{a^o_{Ca^{2+}} a^o_{C_2O_4^{2-}}}{P_s} - 1 \tag{14}$$

Corresponding activity coefficients are estimated from the Guggenheim relation (Robinson and Stokes, 1959).

Current total concentrations in calcium and oxalate are given by:

$$T_{Ca} = C_{Ca^{2+}} + C_{CaC_2O_4}$$

and

$$T_{C_2O_4} = C_{C_2O_4^{2-}} + C_{CaC_2O_4} \tag{15}$$

and the current mean supersaturation:

$$S = \frac{a_{Ca^{2+}} a_{C_2O_4^{2-}}}{P_s} - 1 \tag{16}$$

Defining the conversion X as:

$$T_{Ca} = T^o_{Ca} - (T^o_{Ca} + T^o_{C_2O_4})X$$

and

$$T_{C_2O_4} = T^o_{C_2O_4} - (T^o_{Ca} + T^o_{C_2O_4})X \tag{17}$$

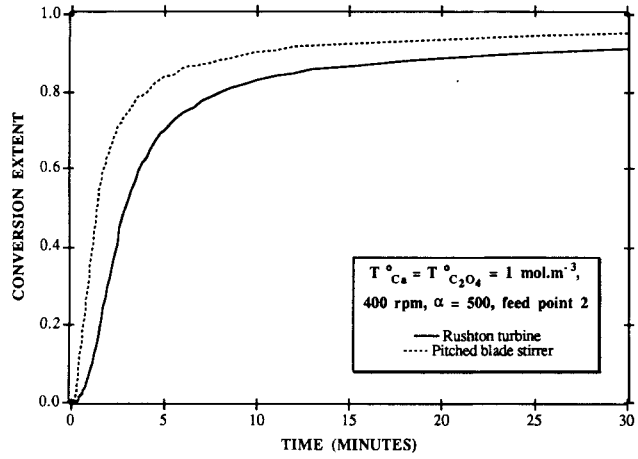

Figure 6a. Extent of conversion as a function of time for two stirring mobile types.

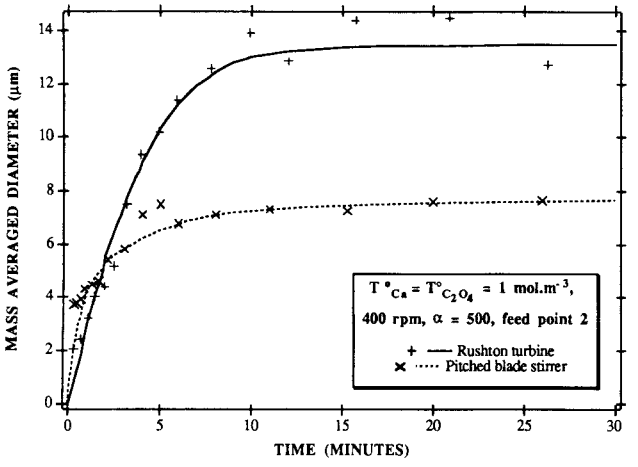

Figure 6b. Mass-averaged diameter as a function of time for two types of stirring mobile.

the experimental conductivity of the solution γ is related to X through the following expression:

$$\gamma = 2T^{o}_{Ca}\Lambda_{CaCl_2} + 2T^{o}_{C_2O_4}\Lambda_{K_2C_2O_4} - 2\{(T^{o}_{Ca} + T^{o}_{C_2O_4})X + C_{CaC_2O_4}\}\Lambda_{CaC_2O_4} \quad (18)$$

where Λ_{AB} is estimated using the Falkenhagen, Leist and Kelbg relationship associated with Güntelberg's assumption (Robinson and Stokes, 1959):

$$\Lambda_{AB} = \left(\Lambda^{o}_{AB} - \frac{10^7\mathfrak{F}^2}{6\pi\eta\mathfrak{N}_A}(z_1+z_2)\frac{K}{1+\sqrt{I}}\right) \times \left(1 - \frac{z_1z_2e^2}{3\epsilon k_BT}\frac{q}{1-q}\frac{K}{\sqrt{I}(1+\sqrt{I})}[\exp\{\sqrt{I}(1-\sqrt{q})\}-1]\right) \quad (19)$$

with

$\Lambda^{o}_{AB} = \lambda^{o}_1 + \lambda^{o}_2$, equivalent conductivity of $(A^{z1}_{v1}B^{z2}_{v2})$ electrolyte at infinite dilution,

$$K = \frac{8\pi\mathfrak{N}_A e^2 I}{1{,}000\ \epsilon k_B T}$$

and

$$q = \frac{z_1z_2(\lambda^{o}_1 + \lambda^{o}_2)}{(z_1+z_2)(z_2\lambda^{o}_1 + z_1\lambda^{o}_2)}$$

The solution of Eqs. 18 and 19 is obtained by a numerical optimization procedure. Then, current concentrations $C_{Ca^{2+}}$, $C_{C_2O_4^{2-}}$, and $C_{CaC_2O_4}$ derive from Eqs. 11, 15 and 17.

When the concentration of solid is high enough to alter conductivity measurements, γ has to be corrected by means of the Neale's Formula (Neale and Nader, 1973).

Solid phase

Evolution of the solid phase is followed by automatic periodic sampling of the suspension (every 5 seconds at the beginning of the precipitation if necessary). To quench the reaction, samples are immediately diluted by an appropriate volume of electrolytic solution. So as to prevent any further redissolution of the samples this dilution medium is previously saturated with respect to calcium oxalate and filtered through a 0.22-μm pore-size membrane.

A Coulter counter fitted with a 100-μm orifice tube was used to determine the corresponding CSD's. The samples were carefully treated by ultrasonic dispersion before the particle size analysis to destroy artificial agglomerates that may occur. Recovery of the crystals by filtering the samples on 0.22-μm membrane filters makes it possible to carry out qualitative investigations by the scanning electron microscopy or X-ray diffractometry. This allows crystal morphology and composition to be studied as a function of time.

Experimental Results

The investigation was specially concerned with the following four parameters: initial total concentrations, type of stirrer, stirrer speed, and feed point location.

Variation of the total initiation concentration

Figures 5a (liquid phase) and 5b (solid phase) show the results of the four experiments involving different initial total concentrations and the same fluid mixing characteristics (Rushton turbine, 600 rpm, $\alpha = 250$, feed point 2).

As expected, for the case of equimolar solutions, the higher the initial total concentration, the higher the reactant consumption and crystal growth rates. Reaction times are greatly affected by this parameter: 80% conversion requires 45 seconds for 2 mol·m^{-3}, 6 minutes for 1 mol·m^{-3}, and 48 minutes for 0.5 mol·m^{-3}.

In the case of nonequimolar solutions, the behavior lies between the two equimolar precipitations corresponding to the lower and the higher concentration, respectively.

Changing the type of stirrer mobile

Experiments with a Rushton turbine and a four-bladed 45-degree-angle pitched stirrer have been carried out under identical precipitation conditions (initial total concentrations 1 mol·m^{-3} equimolar, 400 rpm, $\alpha = 500$, feed point 2). Figures 6a and 6b present the corresponding changes in the liquid and solid phases. The main observation is that with respect to the Rushton turbine, mixing with the pitched-blade stirrer in-

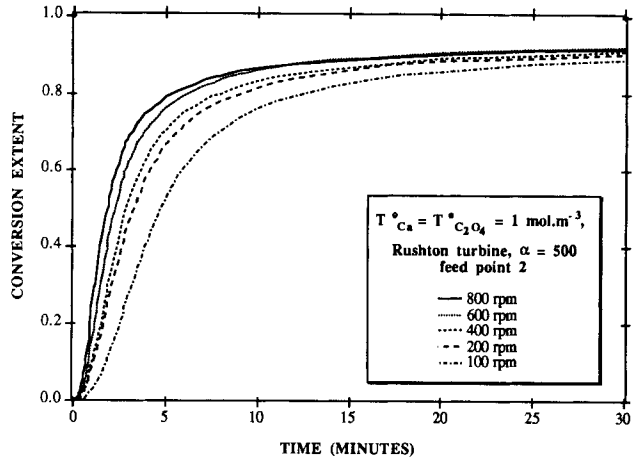

Figure 7a. Extent of conversion as a function of time for several stirring speeds.

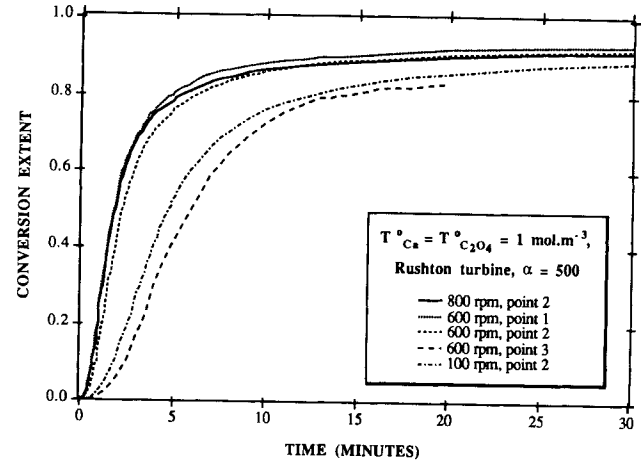

Figure 8a. Conversion extent as a function of time for different addition points.

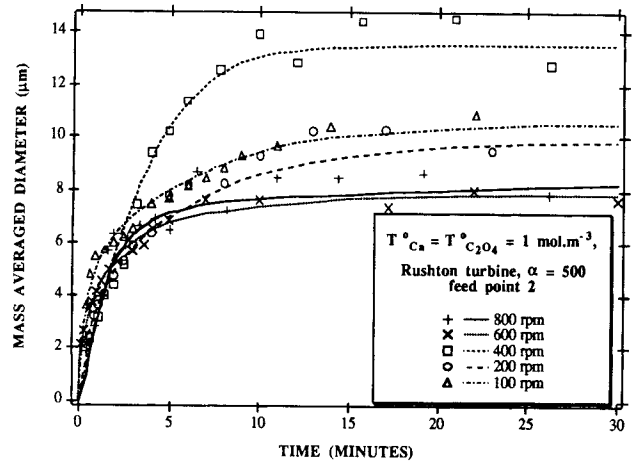

Figure 7b. Mass-averaged diameter as a function of time for several stirring speeds.

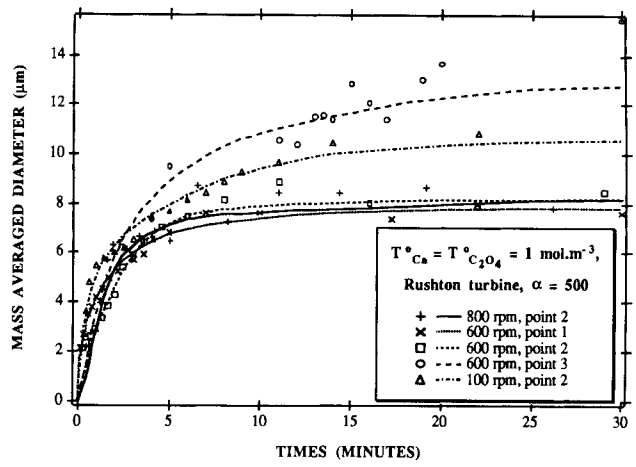

Figure 8b. Mass-averaged diameter as a function of time for different addition points.

creases the overall crystallization rate r and produces more crystals of smaller size.

Variation of the stirring speed

Similar calcium oxalate precipitations (1 mol·m^{-3} equimolar, Rushton turbine, $\alpha = 500$, feed point 2) have been performed at various stirring speeds and are given on Figures 7a and 7b. The most significant trends are that the overall crystallization rate r increases with the stirring speed, while the mean crystal diameter D shows an apparently variable dependence on this factor.

These experimental conclusions correspond to the predictions of our previous model: at the same feed point, increasing the stirring speed increases the overall crystallization rate, but have uncertain effects on N_c and D (Table 1, first case).

Modification of the feed point location

Using the same operating parameters (1 mol·m^{-3} equimolar, Rushton turbine, 600 rpm, $\alpha = 500$), experiments have been performed using various feed point locations (Figures 8a and 8b). These are numbered in the order of the decreasing level of turbulence (Figure 1).

Experimental tendencies are consistent with the predictions of the model: at the same stirring speed, addition of calcium chloride solution in a more turbulent zone leads to a higher overall crystallization rate, and a greater number of crystals of smaller size (Table 1, second case).

Extreme curves resulting from variations of the stirring speed with the feed point 2 have also been reported on the same figures. Comparatively, they demonstrate that the choice of addition point is more important than that of stirring speed as far as mixing effects are concerned.

It is also noted that modification of the feed point location only affects the first second of the mixing and the primary nucleation, whereas complete precipitation occurs over the period of several minutes. Thus, even such a short time interval is sufficient to change the crystal size distribution and the concentration profiles vs. time.

Use of the micromixing model to reduce the influence of mixing

As shown previously, the feed point location is the most sensitive factor with regard to the influence on micromixing. Therefore, when hydrodynamics are found to affect a precip-

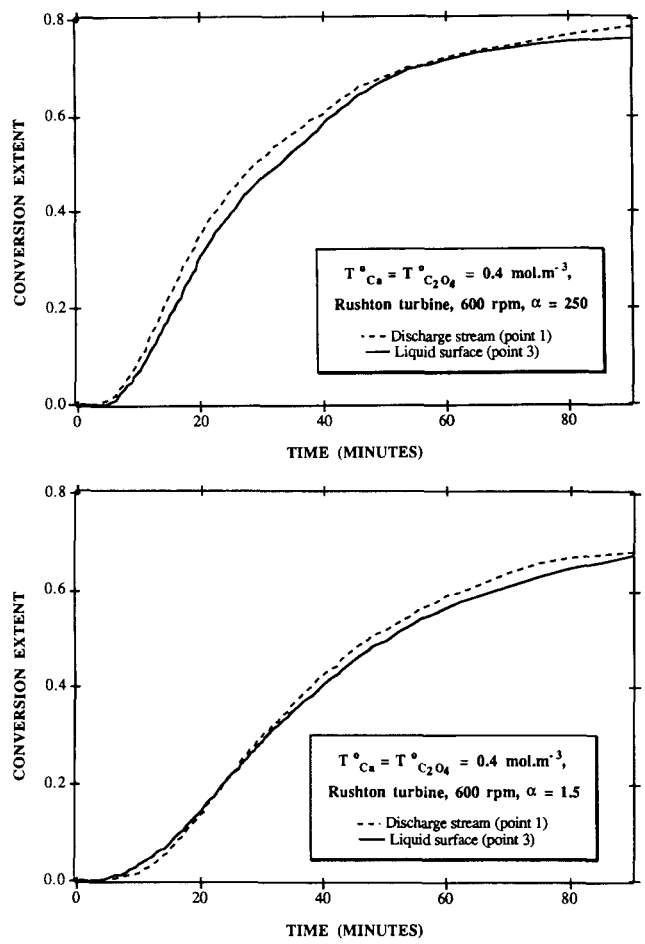

Figure 9a. Conversion extent as a function of time for extreme addition point and two values of α.

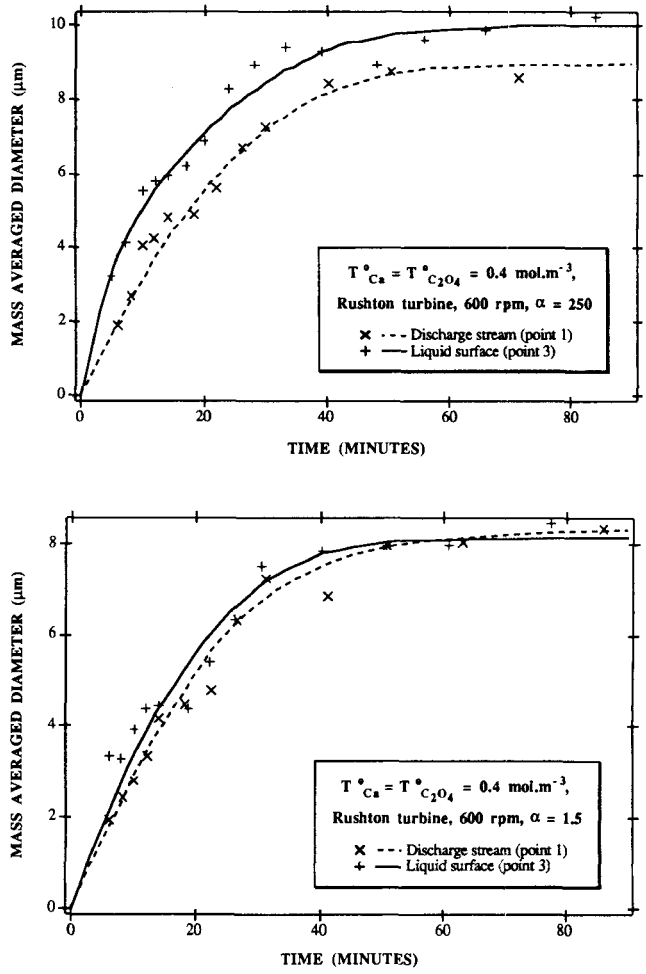

Figure 9b. Mass-averaged diameter as a function of time for extreme addition points and two values of α.

itation process, the greatest differences in overall crystallization rate and CSD will be observed for the case of an addition point located near the liquid surface and one in the discharge stream close to the stirrer (feed points 3 and 1).

We have investigated the efficiency of using low α values on the basis of this qualitative test of mixing and according to the deductions given previously. Thus, we performed experiments at two α values: 250 and 1.5 with the following conditions kept constant (0.4 mol·m^{-3} equimolar, Rushton turbine, 600 rpm). Experiments were repeated at each of the two previously identified limiting cases for the addition point location to emphasize micromixing effects.

Whereas r seems to be slightly affected by a change in α (Figure 9a), D exhibits a strong dependence on this parameter (Figure 9b). In fact, for an α value of 250, D is greatly affected by the mixing conditions and practically unaffected for an α value of 1.5, and this leads to the conclusion that micromixing effects are then almost absent.

These experimental results support the validity of the conclusions from our model: performing a batch precipitation with a volume ratio α close to unity makes it possible to prevent micromixing interactions.

Conclusions

The simplified micromixing model proposed in this article assumes that primary nucleation is the only precipitation process significantly affected by the hydrodynamics. The volume of solution added to cause precipitation is taken to be perfectly mixed with an increasing fraction α of the initial contents of the reactor. It leads to the following important points:

- Micromixing effects are almost eliminated in a batch precipitator when an overall volume mixing ratio α close to unity is used.
- Mixing interactions are drastically accentuated in semibatch or batch systems with high α values.
- Changes in the feed point location are much more important for micromixing effects than modifications to the stirrer speed.

These predictions have been successfully validated by experimental observations on batch precipitation of calcium oxalate monohydrate. In addition, moving the feed point from one zone to another with a higher turbulence level has been established as a test of the efficiency of micromixing. This indicates that changes in precipitation processes by hydrodynamic factors can now be qualitatively demonstrated.

Acknowledgment

The authors are indebted to Rhône-Poulenc Industrialisation for

financial support and to Miss J. Mutel for assistance in experimental manipulations.

Notation

a = activity, $mol \cdot m^{-3}$
A_N = constant, Eq. 7
B_N = constant, Eq. 7
C = concentration, $mol \cdot m^{-3}$
e = proton charge, C
$\mathfrak{F}$ = Faraday, $C \cdot eq^{-1}$
I = ionic strength, $mol \cdot m^{-3}$
k_B = Boltzman constant, $J \cdot deg^{-1} \cdot mol^{-1}$
K_A = association constant, $m^3 \cdot mol^{-1}$
D = mass averaged diameter, m
m = number of fractions of added volume
$\mathfrak{N}_A$ = Avogadro number, $no \cdot mol^{-1}$
N_c = number of crystals per unit volume, $no \cdot m^{-3}$
P_s = solubility product, $mol^2 \cdot m^{-6}$
r = overall reaction rate
r_N = overall nucleation rate, no. $nuclei \cdot m^{-3} \cdot s^{-1}$
$\underline{S^o}$ = initial local supersaturation
S^o = initial mean supersaturation
T = absolute temperature, K
T_z = total concentration in species Z, $mol \cdot m^{-3}$
V = volume, m^3
X = reaction conversion
Y = ratio, Eq. 6

Greek letters

α = overall volume mixing ratio
β = initial contacting volume ratio
ϵ = dielectric constant
γ = solution conductivity, $S \cdot m^{-1}$
η = kinematic viscosity, $Pa \cdot s$
λ = ionic conductivity, $S \cdot m^2 \cdot mol^{-1}$
Λ = molar conductivity, $S \cdot m^2 \cdot mol^{-1}$
ζ = nucleation efficiency

Subscripts

A = reactant A
B = reactant B

Superscripts

i = initial value before addition
o = initial value after complete and perfect mixing (concentrations, supersaturations); value corresponding to infinite dilution (conductivities)
$*$ = saturation value

Literature Cited

Aslund, B., and A. C. Rasmuson, "An Applied Study of Batch Reaction Crystallization," *Industrial Crystallization 87*, Elsevier, Amsterdam (1989).

Baldyga, J., and J. R. Bourne, "A Fluid Mechanical Approach to Turbulent Mixing and Chemical Reaction: II. Micromixing in the Light of Turbulence Theory," *Chem. Eng. Commun.*, **28**, 243 (1984).

Baldyga, J., and J. R. Bourne, "Simplification of Micromixing Calculations: I. Derivation and Application of New Model," *Chem. Eng. J.*, **42**, 83 (1989).

Baldyga, J., R. Pohorecki, W. Podgorska, and B. Marcant, "Micromixing Effects in Semibatch Precipitation," *Symp. on Industrial Crystallization*, Garmisch-Partenkirchen (1990).

Becker, G. W., and M. A. Larson, "Mixing Effects in Continuous Crystallization," *AIChE Symp. Ser.*, **65**, 14 (1969).

Beek, Jr., J., and R. S. Miller, "Turbulent Transport in Chemical Reactors," *AIChE Symp. Ser.*, **55**, 23 (1959).

Brecevic, L., D. Skrtic, and J. Garside, "Transformation of Calcium Oxalate Hydrates," *J. Cryst. Growth*, **74**, 399 (1986).

Danckwerts, P. V., "The Effect of Incomplete Mixing on Homogeneous Reactions," *Chem. Eng. Sci.*, **8**, 93 (1958).

David, R., and J. Villermaux, "Interpretation of Micromixing Effects on Fast Consecutive-Competing Reactions in Semibatch Stirred Tanks by a Simple Interaction Model," *Chem. Eng. Commun.*, **54**, 333 (1987).

David, R., and J. Villermaux, "Interpretation of Micromixing Effects on Fast Consecutive-Competitive Reactions in Semibatch Stirred Tanks by a Simple Interaction Model," *Chem. Eng. Commun.*, **78**, 233 (1989).

Desai, R. M., J. W. Rachow, and D. C. Timm, "Collision Breeding: a Function of Crystal Moments and Degree of Mixing," *AIChE J.*, **20**, 43 (1974).

Fitchett, D. E,. and J. M. Tarbell, "Effect of Mixing on the Precipitation of Barium Sulfate in an MSMPR Reactor," *AIChE J.*., **36**, 511 (1990).

Gardner, G. L., "Nucleation and Crystal Growth of Calcium Oxalate Trihydrate," *J. Cryst. Growth*, **30**, 158 (1975).

Garside, J., "Industrial Crystallization from Solution," *Chem. Eng. Sci.*, **40**, 3 (1985).

Garside, J., and N. S. Tavare, "Mixing, Reaction and Precipitation: Limits of Micromixing in an MSMPR Crystallizer," *Chem. Eng. Sci.*, **40**, 1485 (1985).

Kuboi, R., M. Harada, J. M., Winterbottom, A. J. S. Anderson, and A. W. Nienow, "Mixing Effects in Double-Jet and Single-Jet Precipitation," *World Congress III of Chem. Eng.*., Tokyo, Paper 8g-302, II, 1040 (1986).

Kulov, N. N., E. K. Nikolaishvili, V. M. Barabash, L. N. Braginsky, V. A. Malyusov, and N. M. Zhavoronkov, "Dissolution of Solid Particles Suspended in Agitated Vessels," *Chem. Eng. Commun.*, **21**, 259 (1983).

Marchal, P., R. David, J. P. Klein, and J. Villermaux, "Crystallization and Precipitation Engineering: I. an Efficient Method for Solving Population Balance in Crystallization with Agglomeration," *Chem. Eng. Sci.*, **43**, 59 (1988).

Matz, G., "Ostwald Ripening—a Modern Concept," *Ger. Chem. Eng.*, **8**, 225 (1985).

Mersmann, A., and M. Kind, "Chemical Engineering Aspects of Precipitation from Solution," *Chem. Eng. Technol.*, **11**, 264 (1988).

Neale, G. H., and W. K. Nader, "Prediction of Transport Processes within Porous Media: Diffusive Flow Processes within an Homogeneous Swarm of Spherical Particles," *AIChE J.*, **19**, 112 (1973).

Nyvlt, J., O. Söhnel, M. Matuchova and M. Broul, *Kinetics of Industrial Crystallization*, Amsterdam (1985).

Nyvlt, J., and M. Karel, "Crystal Agglomeration," *Cryst. Res. Technol.*, **20**, 173 (1985).

Pohorecki, R, and J. Baldyga, "The Use of a New Model of Micromixing for Determination of Crystal Size in Precipitation," *Chem. Eng. Sci.*, **38**, 79 (1983).

Pohorecki, R,. and J. Baldyga, "The Effects of Micromixing and the Manner of Reactor Feeding on Precipitation in Stirred Tank Reactors," *Chem. Eng. Sci.*, **43**, 1949 (1988).

Robinson, R. A,. and R. H. Stokes, *Electrolyte Solutions*, 2nd ed., Butterworths, London (1959).

Söhnel, O., and J. W. Mullin, "Influence of Mixing on Batch Precipitation,' *Cryst. Res. Technol.*, **22**, 1235 (1987).

Tavare, N. S., "Mixing in Continuous Crystallizers," *AIChE J.*, **32**, 705 (1986).

Tomazic, B. B., and G. H. Nancollas, "A Study of the Phase Transformation of Calcium Oxalate Trihydrate-Monohydrate," *Invest. Urol.*, **16**, 329 (1979).

Tosun, G., "Effect of Addition Mode and Mixing Intensity on Particle Size Distribution in Borium Sulfate Precipitation," AIChE Meeting, San Francisco (1989).

Villermaux, J., and R. David, "Effect du Micromélange Sur la Précipitation," *J. Chim. Phys.*, **85**, 273 (1988).

Appendix: New Approach to Conductivity Analysis and Its Application to the Precipitation of Calcium Oxalate

Theoretical basis

Conductivity reflects the concentration of the ionic species

present in solution. In our experiments involving potassium oxalate and calcium chloride at approximately pH ≅ 7, the species Ca^{2+}, $C_2O_4^{2-}$, K^+, and Cl^- have to be considered.

Let us define the following variables:

γ = overall conductivity of the solution

Λ_{CaCl_2}, $\Lambda_{K_2C_2O_4}$, $\Lambda_{CaC_2O_4}$ = molar conductivities of calcium chloride, potassium oxalate and calcium oxalate

$\lambda_{Ca^{2+}}$, $\lambda_{C_2O_4^{2-}}$, λ_{K^+}, λ_{Cl^-} = ionic conductivities of Ca^{2+}, $C_2O_4^{2-}$, K^+ and Cl^- ions

From the definitions,

$$\Lambda_{CaCl_2} = \lambda_{Ca^{2+}} + \lambda_{Cl^-} \tag{A1}$$

$$\Lambda_{K_2C_2O_4} = \lambda_{K^+} + \lambda_{C_2O_4^{2-}} \tag{A2}$$

$$\Lambda_{CaC_2O_4} = \lambda_{Ca^{2+}} + \lambda_{C_2O_4^{2-}} \tag{A3}$$

The overall conductivity is related to ionic conductivities through:

$$\gamma = 2C_{Ca^{2+}}\lambda_{Ca^{2+}} + 2C_{C_2O_4^{2-}}\lambda_{C_2O_4^{2-}} + C_{K^+}\lambda_{K^+} + C_{Cl^-}\lambda_{Cl^-} \tag{A4}$$

Since K^+ and Cl^- ions are not consumed by the reaction, from relations 15 and 17:

$$C_{K^+} = 2T^\circ_{C_2O_4} \tag{A5}$$

$$C_{Cl^-} = 2T^\circ_{Ca} \tag{A6}$$

$$C_{Ca^{2+}} = T^\circ_{Ca} - (T^\circ_{Ca} + T^\circ_{C_2O_4})X - C_{CaC_2O_4} \tag{A7}$$

$$C_{C_2O_4^{2-}} = T^\circ_{C_2O_4} - (T^\circ_{Ca} + T^\circ_{C_2O_4})X - C_{CaC_2O_4} \tag{A8}$$

Replacing Eq. A4 and using Eqs. A1, A2 and A3:

$$\gamma = 2T^\circ_{Ca}\Lambda_{CaCl_2} + 2T^\circ_{C_2O_4}\Lambda_{K_2C_2O_4} - 2\{(T^\circ_{Ca} + T^\circ_{C_2O_4})X + C_{CaC_2O_4}\}\Lambda_{CaC_2O_4} \tag{A9}$$

The main trouble is then to estimate the molar conductivities Λ_{CaCl_2}, $\Lambda_{K_2C_2O_4}$, and $\Lambda_{CaC_2O_4}$, which depend essentially on electrolyte concentrations.

Former approximate method

The most widely used procedure assumes that concentration of the electrolyte has no influence on molar conductivities, which are therefore constant.

In the case of calcium oxalate precipitation, let us consider the following values:

γ° = initial overall conductivity of the solution

γ^* = overall conductivity of the solution at saturation

Applying the previous assumptions in Eq. A9 leads to:

Table A1. Experimental Ionic Conductivities

Temp. °C	$\lambda^\circ_{Ca^{2+}}$ mS·m²·mol⁻¹	$\lambda^\circ_{C_2O_4^{2-}}$ mS·m²·mol⁻¹	$\lambda^\circ_{K^+}$ mS·m²·mol⁻¹	$\lambda^\circ_{Cl^-}$ mS·m²·mol⁻¹	ϵ	η Pa·s
10	41.43	51.40	53.12	54.38	84.15	$1.307\ 10^{-3}$
11	42.57	52.50	54.40	55.75	83.74	$1.271\ 10^{-3}$
12	43.62	54.05	55.72	57.19	83.37	$1.235\ 10^{-3}$
13	44.76	55.62	57.08	58.55	82.97	$1.202\ 10^{-3}$
14	45.93	57.10	58.36	59.95	82.60	$1.169\ 10^{-3}$
15	46.98	58.70	59.66	61.41	82.23	$1.139\ 10^{-3}$
16	48.27	60.25	61.12	62.89	81.87	$1.109\ 10^{-3}$
17	49.44	61.75	62.40	64.47	81.47	$1.081\ 10^{-3}$
18	50.70	63.25	63.90	66.00	81.10	$1.053\ 10^{-3}$
19	51.87	64.70	65.12	67.37	80.74	$1.027\ 10^{-3}$
20	53.10	66.23	66.44	68.80	80.36	$1.002\ 10^{-3}$
21	54.33	67.70	67.80	70.17	80.02	$9.779\ 10^{-4}$
22	55.71	69.25	69.16	71.71	79.65	$9.548\ 10^{-4}$
23	56.97	70.78	70.48	73.25	79.25	$9.325\ 10^{-4}$
24	58.23	72.47	71.96	74.72	78.89	$9.111\ 10^{-4}$
25	59.50	74.15	73.50	76.35	78.54	$8.904\ 10^{-4}$
26	60.87	75.95	74.90	77.80	78.16	$8.705\ 10^{-4}$
27	62.16	77.75	76.40	79.34	77.81	$8.513\ 10^{-4}$
28	63.60	79.55	77.92	80.95	77.44	$8.327\ 10^{-4}$
29	65.01	81.40	79.32	82.46	77.09	$8.148\ 10^{-4}$
30	66.33	83.30	80.84	84.10	76.77	$7.975\ 10^{-4}$
31	67.77	85.27	82.28	85.64	76.41	$7.808\ 10^{-4}$
32	69.00	87.25	83.64	87.25	76.06	$7.647\ 10^{-4}$
33	70.47	89.23	85.18	88.93	75.70	$7.491\ 10^{-4}$
34	71.91	91.18	86.56	90.54	75.35	$7.340\ 10^{-4}$
35	73.26	93.03	88.21	92.21	75.03	$7.194\ 10^{-4}$
36	74.76	95.02	89.58	93.97	74.69	$7.052\ 10^{-4}$
37	76.23	97.00	91.00	95.65	74.36	$6.915\ 10^{-4}$
38	77.67	99.00	92.44	97.33	74.02	$6.783\ 10^{-4}$
39	79.14	101.15	93.98	98.94	73.67	$6.654\ 10^{-4}$
40	80.58	103.25	95.44	100.62	73.35	$6.529\ 10^{-4}$

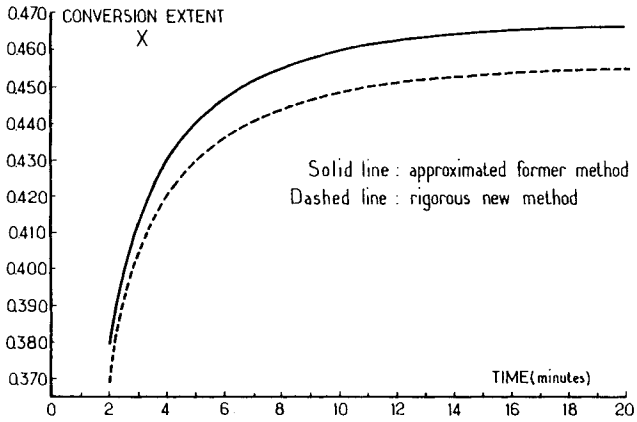

Figure A1. Comparison of the two methods for conductivity analysis.

$$\frac{\gamma^\circ-\gamma}{\gamma^o-\gamma^*}=\frac{(T^\circ_{Ca}+T^\circ_{C_2O_4})X+C_{CaC_2O_4}-C^\circ_{CaC_2O_4}}{(T^\circ_{Ca}+T^\circ_{C_2O_4})X^*+C^*_{CaC_2O_4}-C^\circ_{CaC_2O_4}} \quad \text{(A10)}$$

X^* and $C^*_{CaC_2O_4}$ are easily evaluated from Eqs. 11, 12, 15 and 17. In the general case, $C_{CaC_2O_4}$ is directly related to X through Eqs. 11, 15 and 17. So, the ratio $(\gamma^o-\gamma)/(\gamma^o-\gamma^*)$ depends only on X, and thus straightforward estimation of X is possible.

New rigorous method

Theories of the influence of concentration on the conductivity of the electrolytes originate from interaction concepts, especially electrophoretic and relaxation effects (Robinson and Stokes, 1959).

To evaluate the conductivity of a solution made up of a single electrolyte $A^{z_1}_{\upsilon_1}B^{z_2}_{\upsilon_2}$ dissociating into ions A^{z_1} and B^{z_2},two limiting laws are available, depending on the concentration of the electrolyte.

An expression for the equivalent conductivity of an electrolyte at low concentration was obtained by Onsager in 1927. He neglected the finite size of the ions and assumed their local concentration to be a Boltzmann distribution function, which, together with the electrical potential resulting from the Debye and Hückel theory, gives:

$$\Lambda=\Lambda^o-\frac{z_1z_2e^2}{3\epsilon k_BT}\Lambda^o\frac{qK}{1+\sqrt{q}}-\frac{10^7\mathfrak{F}^2}{6\pi\eta\mathfrak{N}_A}(z_1+z_2)K \quad \text{(A11)}$$

with

$$K^2=\frac{8\pi\mathfrak{N}_Ae^2}{\epsilon k_BT}I \quad \text{(A12)}$$

$$q=\frac{z_1z_2}{z_1+z_2}\frac{\lambda^o_1+\lambda^o_2}{z_2\lambda^o_1+z_1\lambda^o_2} \quad \text{(A13)}$$

$$\Lambda^o=\lambda^o_1+\lambda^o_2 \quad \text{(A14)}$$

$$\Lambda=\lambda_1+\lambda_2 \quad \text{(A15)}$$

Λ^o represents the equivalent conductivity of the electrolyte at infinite dilution, that is, when no electrical interaction occurs between ions in solution. λ^o_1 and λ^o_2 are the ionic conductivities, at infinite dilution, of ions A and B, respectively. I is the driving force of the solution.

When there is a higher concentration of the electrolyte in solution, it is necessary to use the Falkenhagen, Leist and Kelbg expression. In 1952, these authors published an extension of Onsager's theory, taking into account the finite size of ions. Using the Eigen and Wicke assumptions for the electrical potential, they proposed the following expression:

$$\Lambda=\left(\Lambda^o-\frac{10^7\mathfrak{F}^2}{6\pi\eta\mathfrak{N}_A}(z_1+z_2)\frac{K}{1+Ka}\right)\times\left(1-\frac{z_1z_2e^2}{3\epsilon k_BT}\frac{q}{1-q}\frac{K}{Ka(1+Ka)}[\exp\{Ka(1-\sqrt{q})\}-1]\right) \quad \text{(A16)}$$

where a is the closest distance approach of one ion to another ion.

As in Güntelberg's equation describing the activity coefficients of the ions in aqueous solution, we further assume $a=3.04$ Å for all electrolytes at 25°C, resuming in $Ka=\sqrt{I}$. Hence, the earlier expression A16 becomes:

$$\Lambda=\left(\Lambda^o-\frac{10^7\mathfrak{F}^2}{6\pi\eta\mathfrak{N}_A}(z_1+z_2)\frac{K}{1+\sqrt{I}}\right)\times\left(1-\frac{z_1z_2e^2}{3\epsilon k_BT}\frac{q}{1-q}\frac{K}{\sqrt{I}(1+\sqrt{I})}[\exp\{\sqrt{I}(1-\sqrt{q}\}-1]\right) \quad \text{(A17)}$$

In this relation, λ^o_1, λ^o_2, η, and ϵ are unknown variables, which depend essentially on the temperature. As the concentration of the electrolyte is low, the kinematic viscosity η and the dielectric constant ϵ may be taken to be that of water. On the other hand, λ^o_1 and λ^o_2 need to be determined experimentally. In the case of calcium oxalate, the conductivity of known concentrations of calcium chloride and potassium oxalate have been measured as a function of the temperature. Then, using Eq. A17 and a numerical optimization procedure, it is possible to estimate respectively $\lambda^o_{Ca^{2+}}$ and $\lambda^o_{Cl^-}$ with $CaCl_2$ experiments, $\lambda^o_{K^+}$ and $\lambda^o_{C_2O_4^{2-}}$ with $K_2C_2O_4$ ones (Table A1).

These evaluations enable determination of Λ_{CaCl_2}, $\Lambda_{K_2C_2O_4}$ and $\Lambda_{CaC_2O_4}$ at the temperature of the experiment. Then, if γ is accurately measured, X can be derived from Eq. A9 by numerical optimization.

Comparison of the two methods

The first procedure not only neglects the variations of the molar conductivities with the electrolyte concentration, but it also implies an exact knowledge of the final overall conductivity γ^* corresponding to the solubility product P_s. This value is rarely reached exactly at the end of precipitation experiments, since the process becomes slower and slower, resulting in long delays in obtaining the final equilibrium between all the reacting species.

These two assumptions mean that the approximate technique may lead to more than 5% error on estimated values of the extent of conversion when compared to the rigorous method (see the example on Figure A1). In addition, temperature variations are not taken into account here, whereas the second

technique does so by simply using the appropriate values of the ionic conductivities at the appropriate temperature.

Although the rigorous method gives greater accuracy and flexibility, it should be remembered that it requires careful prior experimentation to determine the ionic conductivities as a function of the temperature. The rigorous method can therefore be recommended only for the following cases:

- Fastidious rehearsal experiments
- High precision requirements such as the precise analysis of micromixing effects
- Where the temperature varies with time.

Studies on calcium oxalate precipitation include these three conditions, which is why the new rigorous method was applied for the successful analysis of conductivity measurements.

Manuscript received Nov. 8, 1990, and revision received July 19, 1991.